arXiv:1701.01566v1 [astro-ph.GA] 6 Jan 2017

Periodicity in the continua and broad line curves of a quasar E1821+643

A. Kovačević[1] • L. Č Popović[1,2] • A. I. Shapovalova [3] • D. Ilić [1]

Abstract Here we present an in-depth analysis of the periodicity of the continua and broad emission lines of a quasar E1821+643. We applied non-parametric composite models, the linear sum of stationary and non-stationary Gaussian processes, and quantified contribution of their periodic parts. We found important qualitative differences among the three periodic signals. Periods of ~ 2200 and ~ 4500 days appear in both continua 5100 Å and 4200 Å , as well as in the Hγ emission line. Their integer ratio is nearly harmonic $\sim \frac{1}{2}$, suggesting the same physical origin. We discuss the nature of these periods, proposing that the system of two objects in dynamically interaction can be origin of two largest periods.

Keywords (Galaxies:) quasars: supermassive black holes; Methods: data analysis

1 Introduction

Investigation of active galactic nuclei (AGN) variability overpowers any other observational technique in giving an insight into their structure even on the smallest scales. Among the most interesting related issues is the quest for periodicity, because it could be a signature of supermassive black hole binary (SMBHB, Lobanov & Roland 2002). Periodicity of AGN has been in the spotlight since the work of Sillanpää et al. (1988), where was noticed a regularity in the historical optical light curve of the blazar OJ 287. The large flare events occurred 12 years in the light curve of the blazar, during the period of almost one century of observations.

Up to a few years ago just some AGNs were considered as long-term (or quasi[1]) periodic objects in optical and UV continuum (Hagen-Thorn et al. 2002; Fan et al. 2002; Lainela et al. 1999; Valtonen et al. 2008; Graham et al. 2015a). Graham et al. (2015b) made systematic search for the long-term variations of continuum in large sample of quasars and found more than one hundred candidates. Thorough analysis of these results (see Vaughan et al. 2016) warned community about critical interpretation of derived periodicities. Namely, AGN periodical flux variability may be explained by multiplex and violent physical mechanisms. We list, as an examples, several possibilities (for the first three see Ackermann et al. 2015, and references therein): pulsational accretion flow instabilities; jet precession, jet rotation, helical jet structure; an accretion-outflow coupling mechanism; orbiting disk hot spots (Guilbert et al. 1983). Also, the last two mentioned processes can be presented in SMBHB systems too, distorting and hiding periodic signals. Accordingly, it becomes very important to be able to reveal the periodic signals in AGN time series from the noise that is hiding them.

A. Kovačević

Department of Astronomy, Faculty of Mathematics, University of Belgrade, Studentski trg 16, 11000 Belgrade, Serbia, andjelka@matf.bg.ac.rs, tel 381648650032, fax 381112630151

L. Č Popović

Astronomical Observatory Belgrade, Volgina 7, 11060 Belgrade, Serbia, lpopovic@aob.rs,
Department of Astronomy, Faculty of Mathematics, University of Belgrade, Serbia

A. I. Shapovalova

Special Astrophysical Observatory of the Russian AS, Nizhnij Arkhyz, Karachaevo - Cherkesia 369167, Russia, ashap@sao.ru

D. Ilić

Department of astronomy, Faculty of mathematics, University of Belgrade, Studentski trg 16, 11000 Belgrade, Serbia, dilic@matf.bg.ac.rs

[1]Some models of multiple black hole systems (e.g. Sundelius et al. (1997)) have shown that perturbations in such systems may not have strictly periodic character, so we can think of them as quasi (pseudo) periodic.

Up to now investigations of AGN led to only few non-controversial explanations of SMBHB (e. g. Popović 2012; Bon et al. 2012). Such pseudo-periodic signals can be used in order to predict the epochs of future flux flares within known confidence limits. This would allow us to confirm or discard multiple black-hole candidates and plan future observations based on the expected activity phase of the source.

Among the binary black hole candidates is a quasar E1821+643. Shapovalova et al. (2016), hereafter Paper I, presented the results of the first long-term (1990-2014) optical spectroscopic monitoring of this object. In their study, application of the standard Lomb - Scargle method (LS, Lomb 1976) suggested a possible periodicity in the continuum and broad emission line light curves, which may be caused by orbital motion. Here we extended their periodicity analysis and investigate the signal/red noise distinction in the continua and emission lines time series of this object. We applied composite non-parametric models, i.e. the linear combination of simple Gaussian processes, to the continua at 5100 Å, 4200 Å, Hβ and Hγ emission lines. The aim of this paper is twofold: first, to investigate in depth periodic signals in the light curves of this object and second, to provide more clues on its broad line region (BLR) geometry and its possible SMBHB nature.

A short description of used observations and insight into Gaussian processes are presented in the section Data sets and Methods. In the section Results and Discussion we display Gaussian processes models of our light curves, their inferred periods and discuss their implications on rough geometrical characteristics of BLR of E1821+643.

2 Data sets and Methods

We examine four diverse time series containing the integral fluxes of the broad Hβ, Hγ emission lines and the fluxes for the continuum at the rest frame wavelength of 5100 Å and 4220 Å. As the temporal coverage and sampling of data sets are important for an extensive search for a periodic behavior of an AGN, reader can find this analysis in Paper I.

AGN time series are usually sparse and irregularly sampled. Even if each time series is defined over a common continuous time interval, they can be defined on different collection of time points due to irregularity. Also, the distribution of intervals between time points are usually not uniform and the number of observations in different time series can be different. Learning any characteristic in such setting is difficult.

It has been shown that the Gaussian process (GP Rasmussen & Williams 2006) naturally conforms to sparse and irregular sampled time series. GP are suitable to AGN light curves, since in general they are complex and with no simple parametric form available. In such situation our prior knowledge about right model can be limited to some general facts. For example, we may just know that our observations originate from underlying process which is discrete, non-smooth, that has variations over certain characteristic time scales and/or has typical amplitudes. Surprisingly, it arises naturally to work with the infinite space of all functions that have such general characteristics. As these functions are not characterized with explicit sets of parameters, these techniques are called non-parametric modeling. Since the dominant tools for working with such model is probability theory, they are recognized as Bayesian non-parametric models, and particular member of such models are GPs. Moreover, AGN variability amplitude is large and their luminosity is always positive, allowing us to perform calculations using variable l(t) = ln (Flux(t)), which can be assumed to be GP (Nipoti & Binney 2015).

The simplified version of GPs (namely continuous time first-order autoregressive process (CAR(1))) has been used to model AGN continuum light curves (see Pancoast et al. 2014, and reference therein). These works used Ornstein - Uhlenbeck (OU) covariance function:

$$K_{\rm OU}(\Delta t) = \frac{\hat{\sigma}^2}{2\alpha_0} \exp^{-\alpha_0 \Delta t}$$

where $\frac{1}{\alpha_0}$ is characteristic time scale, $\hat{\sigma}^2$ is variance of driving noise, and Δt is the time separating two observations (see Kelly et al. 2014). (Note here that this kernel can be written also in the form

$$K_{\rm OU}(x, x') = \sigma^2 \exp\Big(-\frac{|x - x'|}{l}\Big),$$

where the parameter σ^2 is the variance and l is the characteristic length scale of the process, i. e. how close two points x and x' have to be to influence each other. The OU process is a stationary GP. Since the information about the underlying nature of AGN light curves is crucial for probing their variability, Kelly et al. (2011), Andrae et al. (2013) and Zu et al. (2013) modeled the light curves as a parameterized stochastic process with composite covariance functions. Following the same direction of investigations, we applied some of stationary and non-stationary composite covariance functions. As they are a linear combination of other simpler covariance functions, we are able to incorporate insight about periodicity, red noise and nonstationarity of underlaying processes.

In our research we employed two kind of kernel families: stationary - already mentioned OU precess, the squared exponential (SE):

$$K_{\rm SE}(\Delta t) = \frac{\hat{\sigma}^2}{2\alpha_0}\exp^{-(\alpha_0\Delta t)^2},$$

which alternative representation is

$$K_{\rm SE}(x,x') = \sigma^2\exp\Big(-\frac{||x-x'||^2}{2l^2}\Big),$$

rational quadratic (RQ)

$$K_{\rm RQ}(\Delta t) = \frac{\hat{\sigma}^2}{2\alpha_0}(1+\frac{\alpha_0^2|\Delta t|^2}{\alpha})^{-\alpha},\ \text{with}\,\alpha = 2;$$

with an alternative form

$$K_{\rm RQ}(x,x') = \sigma^2(1+\frac{|x-x'|^2}{\alpha l^2})^{-\alpha}\,\text{with}\,\alpha = 2;$$

non-stationary – the standard periodic kernel (StdPer)

$$K_{\rm StdPer}(\Delta t) = \frac{\hat{\sigma}^2}{2\alpha_0}\exp\Big(-\frac{2\sin^2(\frac{\pi(\Delta t)}{P})}{(\frac{1}{\alpha_0})^2}\Big)$$

with alternative version

$$K_{\rm StdPer}(x,x') = \sigma^2\exp\Big(-\frac{2\sin^2(\frac{\pi(x-x')}{P})}{l^2}\Big);$$

and Brownian motion (Brw, red noise or Wiener process)

$$K_{\rm Brw}(\Delta t) = \frac{\hat{\sigma}^2}{2\alpha_0}\min(\Delta t),$$

which alternative form is

$$K_{\rm Brw}(x,x') = \sigma^2\min(x,x').$$

The SE is infinitely differentiable allowing GP with this covariance function to generate functions with no sharp discontinuities. An alternative to the sum of SE kernels is RQ. It was shown that this kernel is equivalent to summing many SE kernels with different scales. This produces variations with a range of time scales. Parameter α is roughness, it determines the relative weighting of large and small scale variations. Under condition $\alpha \to \infty$, the RQ becomes identical to SE. In StdPer kernel hyper parameters P, l correspond to the period and length scale of the periodic component of the variations. In this case l is related to P so it has no dimension.

We applied Brownian motion because it is, in a certain sense, a limit of rescaled simple random walks. Many stochastic processes behave, at least for long ranges of time, like random walks with small but frequent jumps. The argument above implies that such processes will look, at least approximately, on the proper time scale, like Brownian motion. It is very important when probing the periodicity of light curves, to take into account the red noise. It is often presented in the AGN continuum and broad emission lines. Such noise can produce spurious signals in a power spectrum of periodogram. We point out that 'red noise' variability of AGNs originates in physical processes of the source and it is not result of measurement uncertainties. The red noise simulations were produced by OU process having the variance of real light curves.

Since all of these base kernels are positive semidefinite kernels (i.e. the valid covariance functions can be defined) and closed under addition and multiplication, we can create richly structured and interpretable kernels with their summation and/or multiplication. By summing kernels, data can be modeled as a superposition of independent functions, representing different structures. In the case of our time series models, sums of kernels can express superposition of different processes operating at different scales. Since we are applying these operations to the covariance functions, the composition of even a few base kernels can catch complex relationships in data which are not of simple parametric form. This enable us to search for the structure in our data, i.e. periodicity/red noise, and capture them. We determine the number of probing and valid periods by utilizing so called 'a two tier approach' of Vlachos et al. (2005). On the first tier the period candidates are extracted from the periodogram analysis. On the second tier, these periods are verified by other method (these authors used autocorrelation function). In our case, on the first tier we extracted three candidate periods (see Paper I) by means of periodogram analysis. Here, on the second tier, we put these three candidate periods into composite GP models. If these models provide better modeling result than their non periodic parts and if the optimized values of periods are close to the candidate values (within a few hundred of days) then we can consider these values as a valid periods.

For our analysis, we used the following kernels:

$$\text{SE} + \sum_{\text{i}=1,3}\text{StdPer}_\text{i} \tag{1}$$

$$\text{RQ} + \sum_{\text{i}=1,3}\text{StdPer}_\text{i} \tag{2}$$

$$\text{Brw} + \sum_{\text{i}=1,3}\text{StdPer}_\text{i} \tag{3}$$

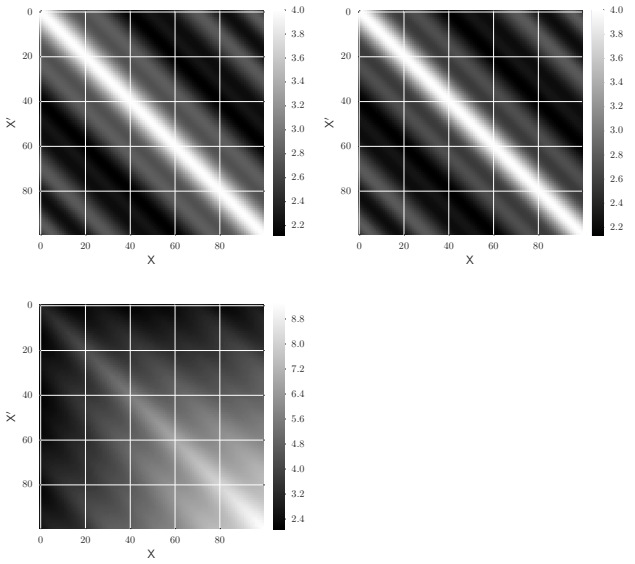

Fig. 1 The prior covariance matrices associated with composite kernels given by equations 1 (top left), 2 (top right), and 3 (bottom) are calculated from 100 artificial equidistant points. The lightest shade indicates the highest and the darkest shade lowest covariance.

where $\mathrm{StdPer_i}, \mathrm{i} = 1, 2, 3$ are periodic kernels for searching for specific periods $\mathrm{Per_i}, \mathrm{i} = 1, 2, 3$.

The structure of above defined kernels' covariances can be visualized by 'heatmap' of the values in the covariance matrix. For demonstration purpose only, arbitrary one dimensional input space has been discretized equally, and the covariance matrices of Eq. 1, 2 and 3 are constructed from this ordered list (see Figure 1). The region of high SE and RQ covariance is depicted as a diagonal white band, reflecting the local stationary nature of these two kernels. Increasing the lengthscale l increases the width of the diagonal band, since points at larger distance from each other become correlated.

Since we summed periodic and non-periodic kernels it is important to quantify the periodicity of inferred composite models. For this purpose, we applied the method of Durrande et al. (2016) for the first time in astronomy. According to their prescription, let y_p and y_a be the periodic and non-periodic components of our model calculated on random variable of input data points. To quantify the periodicity signal, we calculate periodicity ratio as:

$$\mathrm{S} = \frac{\mathrm{Var(y_p)}}{\mathrm{Var(y_p + y_a)}} \tag{4}$$

Furthermore, S cannot be viewed as a percentage of the periodicity of the signal rigorously since $\mathrm{Var(y_p + y_a)} \neq \mathrm{Var(y_p)} + \mathrm{Var(y_a)}$. Consequently, S can have values greater than 1.

For selecting a model from a set of candidate models, which is best supported by our data, the Bayes factor (BF) (Jeffreys 1961; Kass & Raftery 1995) is used. The BF of two models $\mathrm{Model}_i, \mathrm{Model}_b$ is just ratio of their marginal likelihoods $\mathrm{ML(Model}_i)$, $\mathrm{ML(Model}_b)$ derived using the same dataset, and it includes all information about a particular Bayesian model. BF is preferred for model selection criteria because they contain the information about a model prior. For interpreting the values of BFs we used half-units of the logarithmic metric ($\mathrm{LBF} = \log_{10}(\mathrm{BF}) = \log_{10}\mathrm{ML(Model}_i) - \log_{10}\mathrm{ML(Model}_b)$), since we have already calculated the marginal log likelihood of our models. The interpretation of LBF is that when $0 < \mathrm{LBF} < 0.5$, there is an evidence against $\mathrm{Model_i}$ when compared with $\mathrm{Model_b}$, but it is only worth a bare mention. When $0.5 \leq \mathrm{LBF} < 1$ the evidence against $\mathrm{Model_i}$ is definite but not strong. For $1 \leq \mathrm{LBF} \leq 2$ the evidence is strong and for $\mathrm{LBF} > 2$ it is decisive. In our case we will compare models to the base model - red noise $\mathrm{Model_b} = \mathrm{M_{OU}}$ which is generated from OU kernel. Results in this work have been calculated with 1.0.7 version of the Pythonic Gaussian process toolbox GPy (http://github.com/SheffieldML/GPy).

3 Results and Discussion

As our GP models have a number of hyperparameters (the covariance functions are composites, see Table 1), we first assigned a prior values to some of hyper parameters, obtained from our analysis of light curves in Paper I. In assigning informative priors to three periods in our GP models, we used priors of 4500, 2000 and 1400 days (from the LS periodogram analysis), constraining that the most important periods were on the order of thousand days, rather than on larger or smaller scales (e. g. seconds or millennia). So the range of priors to the periods were [0,1400],[0,2000] and [0,4500] days.

From the heteroskedastic OU process and CARMA model (Kelly et al. 2014) random light curves were sampled to a irregular time intervals of real light curves, in order to to test if periodicity found by LS method is the product of random variations. In such a way, we also compare their effects as a base red noise models. The reason for trying this two types of models is a radio-loud, X-ray nature of E1821+643, due to which its light curves may not be well described by OU models. Moreover, Kozlowski (2016) has shown that OU models can be a degenerate descriptors. A CARMA models might serve better for this purpose, particularly as the red noise terms in them can produce quasi-periodicities which are missing from simple OU

models. For the purpose of CARMA modeling we used Brandon Kelly carma_pack Python package available on https://github.com/brandonckelly/carma_pack. CARMA models lightcurve as sum of (deterministic) autoregression plus (random) stochastic noise. The CARMA model order input is optional. We automatically choose the CARMA order (parameters (p,q)) by minimizing the AIC (Aikake Information Criterion). Also, the residuals from the one-step-ahead predictions standardized by their standard deviation were uncorrelated. Random light curves were sampled with built in functions in GPy and farm_pack packages.

We recalculated periods of each real and simulated curve (see Figure 2) by means of Bayesian formalism for the generalized LS periodogram (BGLS Mortier et al. 2015), which gives the probability of signal's existence in the data. It can be seen that powers of BGLS peaks of OU and CARMA 'red noise' curves are asymptotically close to each other as well as to the continua 4200 Å 5100 Å and the Hγ line (Figure 2).

Due to this fact we will consider as base red noise model OU. Also, in our calculations will be included models given by Eq. 3 and

$$\mathrm{PM_K} = \mathrm{K} + \sum_{\mathrm{i}=1,3} \mathrm{StdPer_i}, \mathrm{K} = \mathrm{OU}, \mathrm{Brw}.$$

Models $\mathrm{PM_{OU}}, \mathrm{PM_{Brw}}$ consist of a set of signals ($\mathrm{StdPer_i}$) superimposed on the red noise ($\mathrm{Brw}, \mathrm{OU}$). These models allow us to disentangle signals in the light curves from the 'red noise' background in which they are immersed.

We initially set default hyperparameters of variance to the variance of light curves and lengthscale between 0.5 and 100 days. The variance determines the average distance of our function away from its mean. Initially we expect to have the same variance as our light curves. We chose range of lengthscales between the minumum of sampling times of observations (~ 0.5 days) and twice of mean of sampling times ($\sim$ 100 days). The lengthscale determines the length of the 'wiggles' in our function, so with larger lengthscale than 100 days the function would be smoother.

For each light curve, the values of these parameters are estimated using maximum likelihood. The assigned values of the models parameters may not be relevant for the current data (e. g. the confidence intervals of models can be too wide). So, we optimized them by maximizing the marginal log likelihood of the observations, using Broyden-Fletcher-Goldfarb-Shanno (BFGS) algorithm, which is the option of the GPy tool. It automatically finds a compromise between model complexity and data fit.

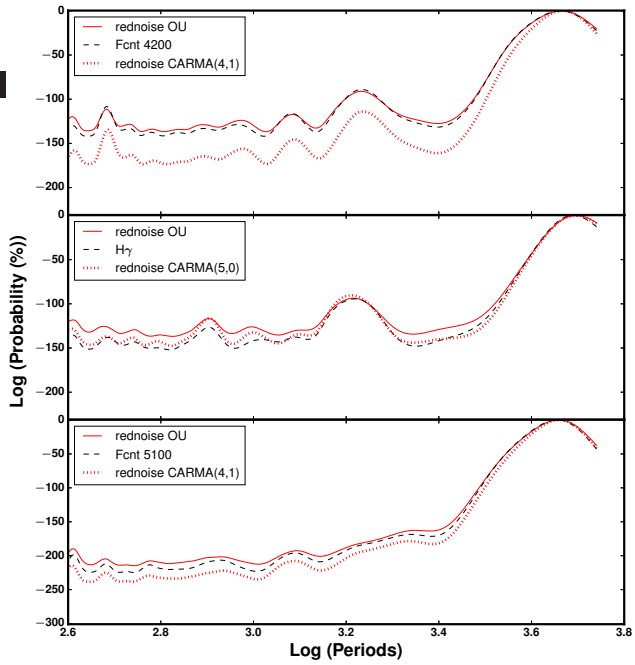

Fig. 2 Bayesian periodograms of the simulated 'red noise' and real light curves on a logscale.

To address the heteroskedasticity of data errors we have applied homoskedastic GP regression on logarithmic transformed dependent variable heteroscedastic GPy regression on non-transformed data. Both methods provide almost the same results, which is clearly seen in the case of three periodic composite models (Table 1 and Table 2).

The one periodic component models (Table 3) are not favored since S are large while LBF are small and vice versa for heteroscedastic regression (S_{het} are small and LBF_{het} is large). Despite two periodic components models (Table 4) have large S and S_{het} they are not favored since their mean values of LBF and LBF_{het} are smaller than corresponding values in Table 1 and Table 2 respectivelly. So three periodic component models inferred from homoskedastic (Table 1) and heterskedastic regressions (Table 2) are dominant, providing almost the same results.

For simplification purpose and following prescription of Nipoti & Binney (2015), we will refer on the results from Table 1 in further discussion.

In Table 1, we compare and contrast quantitatively how well each model captured the pattern of periodicity and random noise of each light curve. Before any quantification of the difference between models, from simple visual inspection of Figure 3 can be seen that there is more uncertainty around the predictions of $\mathrm{M_{OU}}$ then other models. Actually, in regions of sparse

data, the predictive distribution is unchanged from the prior, whereas in data dense regions, the uncertainty is smaller. This suggests worse performance of GP without periodic components. The predictions improve notably as more structure is added to models (i. e. periodic kernels). The similar characteristics, but not so pronounced, can be seen in the models of continuum 4200 Å (Figure 4). Also, Table 1 shows that even from combination of three periodic kernels the learned model will select two periods. This is not the case when we used M_1, M_2 models for the continuum 5100 Å and $PM1_{OU}$ model for the continuum 4200 Å. Perhaps explanation lies in the very nature of these signals (i.e. the shortest periodic signal is weakest).

None of our composite models were able to represent the Hβ line. An example of such failure is depicted on Figure 6. We attribute it to the loss of periodic signal. Furthermore, in Paper I was shown that the time delay of Hβ is larger than the Hγ emission line, meaning that the Hβ line originates at larger radii than Hγ. Combining previous facts (failure of Hβ modeling and its larger distance of origin), it seems that at the Hβ line distance some chaotic processes can exist (like outflows) destroying all periodic signals. We discuss reasons for this scenario in the Section 3.1.

Moreover our learned models did not select a single period which is the least common multiple of three (or two larger) periods. This fact shows that such model with one period cannot reproduce the light curves while the models with two periods can produce them very well. The results imply that the contributions from the two periods are significant, and the flare-lake events reported in Paper I are not random but have the same physical origin.

The contribution of periodic part of each model is estimated with the ratio S given by Eq. 4. For all models the periodic part is strong ($S \geq 1$). We emphasize that flare like events are associated with GP mean curve, which ensures that the behavior of the GP models cannot simply be interpreted as overfitting due to added periodic kernels. Also, Table 1 shows that the LBF exhibited preference for the models with periodic parts. Factor values larger than 2 on the $\log_{10}$ scale gives decisive evidence in favor of composite models (with periodic parts). Thus, all models (except M_3) expressed decisive evidence in favor of composite models. However, M_3 model of Hγ (Figure 5) and the continuum 5100 Å still indicate that the data express substantial to strong evidence in favor of composite models. The mean periods averaged over all models are given in MP row of Table 1. The shortest value of averaged periods is comparable with the consecutive intervals between 4 peaks in R band photometric light curve found in Paper I (see their Fig.1). While medium period almost equals the intervals between the first flare and third, and second and last flare. The largest period is somewhat greater than the interval between the first and the last flare in R band curve since its monitoring period is shorter than optical spectroscopic light curves. However it equals the interval between the two local maximum in optical fluxes observed around MJD 51500 and 56000 (see Figure1-3,5 in Paper I). Association of $\sim$ 4500 days period with ocurence of two local maximum in optical light curves as well as its comensurable relation with period of $\sim$ 2200 days indicate its physical relevance, despite of observational coverage of 5700 days (see Vaughan et al. 2016, for statistical conditions of reliable period detection).

3.1 The nature of periodicity in E1821+643

Here we will analyze possible physical origin of inferred periods. It is interesting to see do we have enough information to discern whether the detected periods can arise from the orbital motion of distinct sources of radiation (such as bright spots) within the accretion disk or distinct physical objects in mutual dynamical interaction (which can be also binary black hole system). Through variety of numerical simulations it has been determined that configurations of SMBH binaries assume circumsecondary ("mini") disk around secondary component, beside circumbinary disk. Also, there are scenarios where mini-disk is seen as the main source of the emission. One of signature of mini-disk presence would be ripples and/or oscillations in the broad FeKα line as suggested by McKernan et al. (2013). However, these signatures will be possible to detect with future observational missions. The numerical study of Noble et al. (2012) shown that if the accretion rate to the inner regions of circumbinary disk were comparable to that of ordinary AGN, the surface density, and therefore the luminosity, of such a circumbinary disk could approach AGN level. Most strikingly, the luminosity should be modulated periodically at a frequency determined by the binary orbital frequency and the binary mass ratio. Since E1821+643 is one of the most luminous quasars and we detected periodical signals in optical light curves, we will put our discussion within the scenario of luminous circumbinary disk, being aware of other possibilites.

The reason to consider the first possibility is that broad line profiles of this object have unusual shapes (thorough line shape analysis is given in Paper I). If the accretion disk is non-axisymmetric, changes in the line shapes will be caused by the disk features orbiting on dynamical time scales. The dynamical time scale (orbital time) of the light emitting region at the radius r of the disk can be approximated by

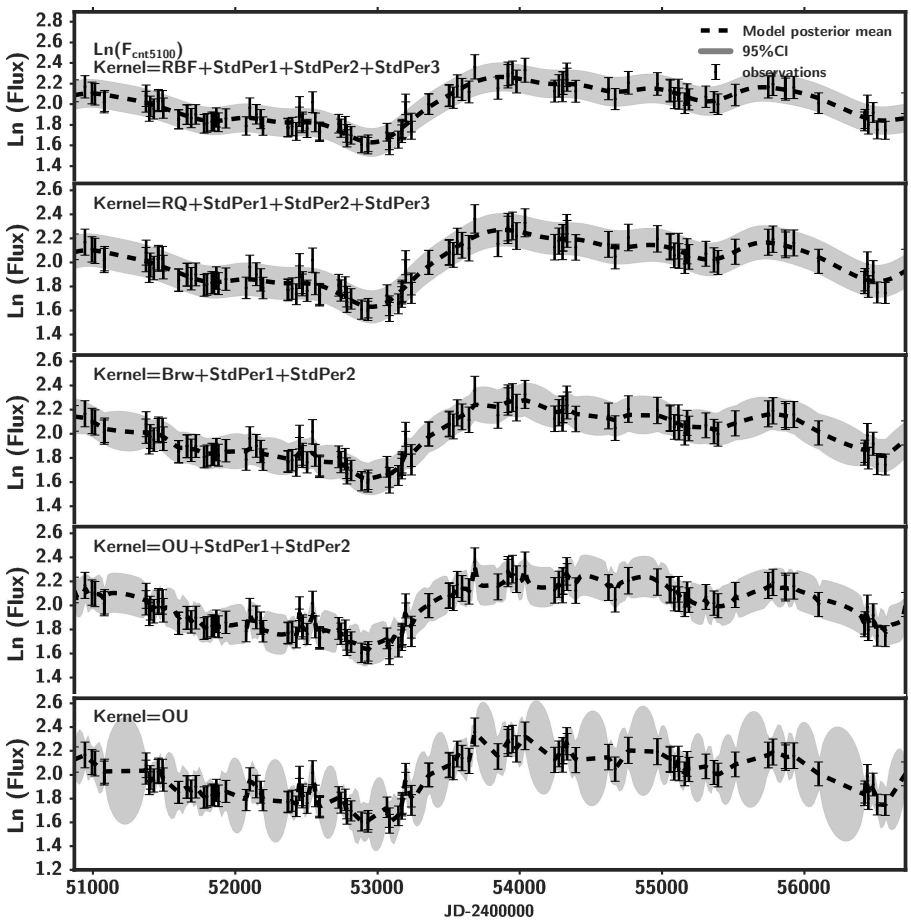

Fig. 3 Comparison of GP posteriors (dashed line - posterior mean function, shaded region - 95% confidence interval) of the continuum at 5100 Å (denoted on each plot as markers with error bars) for different kernel composites. We used natural logarithmic values of fluxes. Composite of Brownian and three periodic kernels provide a richer form of mean function, which explains better data.

$$t_{dyn} \simeq 5 \times 10^{-3} \left(\frac{M}{10^8 M_\odot}\right) \left(\frac{r}{r_g}\right)^{\frac{2}{3}}$$

$$r_g = \frac{GM}{c^2}$$

where $r_g = \frac{GM}{c^2}$ is the gravitational radius around a black hole of mass M, G is the gravitational constant and c the speed of light. By means of this relation we can estimate orbital time of the Hβ and Hγ broad line emitting region. Using their time lags (120 ld for Hβ and 60 ld for Hγ, see Table 10 in Paper I), we estimate that corresponding values of t_{dyn} to their radii of origin are ~ 11.3 yr and ~ 7.1 yr, respectively. These orbital times within the disk are close to two mean largest periods detected by GP (Table 1). However, GP models failed to detect any period in the Hβ line, which prevents us to explain two largest detected periods as the orbital motion within the disk of features such as bright spots. Failure of GP models to extract periods from the Hβ line can be explained by its deterioration. The degree of its disfiguration is easily diagnosed by comparison of the mean profiles of Hβ and Hγ (see Figure 17 in Paper I). The mean Hβ profile exhibits more extended red wing then the mean Hγ. It can be caused by different mechanisms. An additional emission in the far wing of the mean Hβ or even characteristics of observational instruments can result in such degradation of the Hβ line. Also, some processes like outflows can occur within the disk. We recall that Bogdanović et al. (2007) proposed that a black hole ejection should be uncommon in the aftermath of gas-rich mergers. In the gas-rich galactic mergers, torques arising from gas accretion align the spins of supermassive black holes and their orbital axis with a large-scale gas disk. On the other hand, kicking of the black hole may happen espe-

cially in merging galaxies that are relatively gas-poor. So if the kick speed of this object is about the escape velocity of the host galaxy (as reported by Robinson et al. 2010) then we should expect that disk is gas poor and violent processes may contribute to it.

Close similarity between calculated orbital times (t_{dyn} ∼11.3 yr and 7.1 yr, corresponding to the radii of Hβ and Hγ origin within the disk), and two largest periods detected by GP in both continua (at 4200 Å and 5100 Å) and the Hγ line is not decisive factor favoring bright spots within the disk. Because of this we consider another possibility that dynamically related physical objects (which can be also binary black hole system) can cause periodic signals.

Two larger periods (∼ 2200 and ∼ 4500 days, see Table 1) can originate from the real periodic process, because they are related commensurably (their ratio is $\sim \frac{1}{2}$). Information about third signal of ∼ 1700 days is weakly presented in both continua and is absent from Hγ. We note that this period is incommensurate with respect to the two largest periods. It indicates that this signal can be caused by some other process (like flares) within the accretion disk. In such case, 1700 day orbital motion within the disk would correspond to disk's radius of 2 ld.

In the simplest scenario the two largest periods detected by GP can be attributed to the periods of the orbital motion of any two objects in the close mutual dynamical interaction.

Robinson et al. (2010) reported that E1821+643 might be an example of gravitational recoil, while resulting SMBH is moving with velocity of $\sim 2100\,\mathrm{km\,s^{-1}}$. Velocities of such order of magnitude have been found in many theoretical works. For example, Gonzalez et al. (2007) predicted kicks of $\sim 2500\,\mathrm{km\,s^{-1}}$, Campanelli et al. (2007) found kicks velocity up to $\sim 4000\,\mathrm{km\,s^{-1}}$ by means of empirical formula, and Lousto & Zlochower (2009) obtained $\sim 3300\,\mathrm{km\,s^{-1}}$ for nearly maximal spins of black holes in the system. It is believed that configuration, leading to such events (with high velocities kicks), comprises of nearly equal mass circular binaries black holes, with large equal and opposite spins in the orbital plane. Morevover, orbital angular momentum and sum of two black holes' spin-vectors precess around total angular momentum during the in spiral (Barusse and Rezzola, 2009). If the conservation of total angular momentum is valid up to some approximation then the spin and orbital plane precess at the same frequency. In this scenario, we can assume that the precessions of two spin-vectors and orbital angular momentum is ∼ 12 yr , while the orbital period of binary system is ∼ 6 yr (see Table 1). We can use the

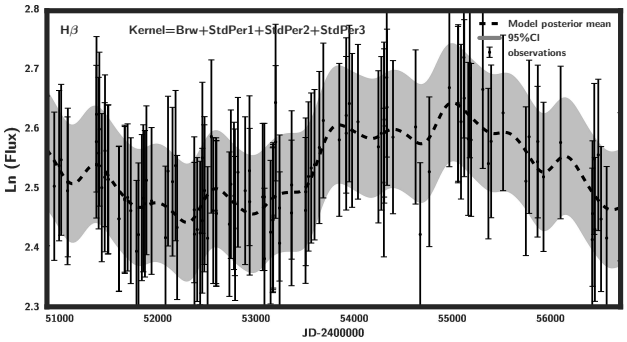

Fig. 6 The same as in Figure 3 but for the H$_\beta$ emission line and just one composite kernel. The shaded area is enlarged around all points, proving that the GP fails to describe daataset. It seems that chaotic processes destroy periodic signals in the Hβ line, preventing GP models to capture any such pattern in the data.

following relation to estimate the rotational period of black hole (see Volvach et al. 2007):

$$\frac{m_1+m_2}{m_2} = \frac{3}{4}\frac{T_{\mathrm{R}} T_{\mathrm{Prec}} \cos\theta}{T_{\mathrm{O}}^2} \tag{5}$$

where m_1, m_2 are masses of two black holes in the system, T_{R} and T_{Prec} are rotational period of black hole and precession period of its orbit, while T_{O} is orbital period. The angle θ is half-angle of the precession cone. Assuming the binaries can be of equal mass $m_1 \sim m_2$, and taking $m_1 + m_2 = 2.6 \times 10^9 M_\odot$ from Paper I, $T_{\mathrm{Prec}} = 12.2$ yr $T_{\mathrm{O}} = 5.8\,\mathrm{yr}$ then we obtain $T_{\mathrm{R}} \sim \frac{7.4}{\cos\theta}$ yr. In close binary system $\cos\theta \sim 1$ since θ converge to small values. It is clear that the period of 4.8 yr (see MP row of Table 1) is not related to the rotational period. This is one more reason to believe that it can originate from the random processes within the disk.

Using the third Kepler's law, we can calculate the radius binary black hole orbit a:

$$\left(\frac{T_{\mathrm{O}}}{1+z}\right)^2 = \frac{4\pi^2 a^3}{G(M+m)} \tag{6}$$

Regaining the value $T_{\mathrm{O}} = 5.8$ yr, we derived $a \sim 6 \times 10^{14}$ m. The upper bound of natural gravitational wave frequency is given by $f_{\mathrm{GW}} < \frac{1}{4\sqrt{2}\pi}\frac{c^3}{GM}$, where M is the mass of the system (Hughes 2003). In our case $f_{\mathrm{GW}} \sim 4.4\times10^{-6}$ Hz. There is no possibility to measure gravitational waves of such low frequency using current ground-based instruments.

Table 3 Comparison of light curve models with one periodic component, using Bayes factor. The names of columns have the same meaning as in Table 1. Subscript $_{het}$ stands for modeling with heteroscedastic errors.

Lc	M	NP	Per [*day*]	ML	S	LBF	NP_{het}	Per_{het}	ML_{het}	S_{het}	LBF_{het}
Cnt_{5100}	M_{OU}[a]	3	-	-125.76	-	-	2	-	119.62	-	-
	PM_{OU}[b]	6	4734	-127.79	1.0	2.02	5	1693	117.95	0.29	-1.66
	M_1[c]	6	2348	-112.289	0.84	-13.48	5	623	110.77	0.68	-8.9
	M_2[d]	7	4529	-126.60	0.63	0.83	6	4500	113	0.63	-6.62
	M_3[e]	5	1160	-126.39	0.62	6.8	4	3519	113.03	0.6	-6.58
Cnt_{4200}	M_{OU}	3	-	-63.41	-	-	2	-	105.76	-	-
	PM_{OU}[b]	6	1841	-64.36	1.18	0.95	5	3532	102.63	0.46	-3.13
	M_1[d]	7	2321	-61.21	1.0	-2.2	6	2419	105.5	0.35	-0.26
	M_2[e]	5	4562	-64.04	0.95	0.63	4	4763	102.04	0.9	-3.36
	M_3[e]	5	4171	-63.79	1.13	0.38	4	4763	102.4	0.62	-3.36
H_γ	M_{OU}	3	-	-56.75	-	-	2	-	31.37	-	-
	PM_{OU}[b]	6	2010	-58.22	1.03	1.47	5	-	-	-	-
	M_1[d]	7	1265	-49.08	4.23	-7.67	6	2196	30.71	0.38	-1.0
	M_2[e]	5	5062	-58.5	1.02	1.75	4	5024	27.62	0.48	-4.09
	M_3[e]	5	4595	-57.38	1.04	0.63	4	4371	29.34	0.54	-2.37

[a] OU model of LC are considered as based model
[b] PM_{OU} assumes $OU + StdPer_i$, $i = 1$
[c] M_1 assumes $SE + StdPer_i$, $i = 1$
[d] M_2 assumes $RQ + StdPer_i$, $i = 1$
[e] M_3 assumes $Brw + StdPer_i$, $i = 1$

Table 4 Comparison of light curve models with two periodic component, using Bayes factor. The names of columns have the same meaning as in Table 1. Subscript $_{het}$ stands for modeling with heteroscedastic errors.

Lc	M	NP	Per_1 [*day*]	Per_2 [*day*]	ML	S	LBF	NP_{het}	Per_{1het} [*day*]	Per_{2het} [*day*]	ML_{het}	S_{het}	LBF_{het}
Cnt_{5100}	M_{OU}[a]	3	-	-	-125.76	-	-	2	-	-	119.62	-	-
	PM_{OU}[b]	9	3784	1760	-126.86	1.06	1.1	8	3573	1154	110.76	0.7	-8.85
	M_1[c]	9	3505	1789	-130.36	1.07	4.59	8	2396	3040	306.94	4.96	187.324
	M_2[d]	10	4744	1607	-128.11	0.63	1.01	9	2903	1682	113.82	0.96	-5.79
	M_3[e]	8	4415	4699	-126.77	0.99	1	7	4827	4722	110.59	0.94	-9.03
Cnt_{4200}	M_{OU}	3	-	-	-63.41	-	-	2	-	-	105.76	-	-
	PM_{OU}[b]	9	3750	1163	-66.09	6.65	2.68	8	3693	1153	101.41	0.59	-4.35
	M_1[c]	10	4890	2373	-63.90	0.99	0.48	9	955	1144	103.23	0.87	-2.53
	M_2[d]	8	4848	2373	-69.72	1.37	6.31	7	4727	-	103.12	0.95	-2.64
	M_3[e]	9	4317	2298	-64.44	1.02	1.03	8	3534	-	102.57	0.53	-3.19
H_γ	M_{OU}	3	-	-	-56.75	-	-	2	-	-	31.37	-	-
	PM_{OU}[b]	9	2648	2081	-60.08	1.03	3.33	8	4509	1124	26.42	0.89	-4.94
	M_1[c]	10	4975	2156	-62.05	0.99	5.30	9	4891	2167	26.04	1.0	-5.33
	M_2[d]	8	4993	2163	-61.91	0.97	5.16	7	4982	2167	26.04	1.0	-5.33
	M_3[e]	9	4975	2156	-62.06	0.99	5.31	8	4982	2167	26.04	0.99	-5.33

[a] OU model of LC are considered as based model
[b] PM_{OU} assumes $OU + StdPer_i$, $i = 1, 2$
[c] M_1 assumes $SE + StdPer_i$, $i = 1, 2$
[d] M_2 assumes $RQ + StdPer_i$, $i = 1, 2$
[e] M_3 assumes $Brw + StdPer_i$, $i = 1, 2$

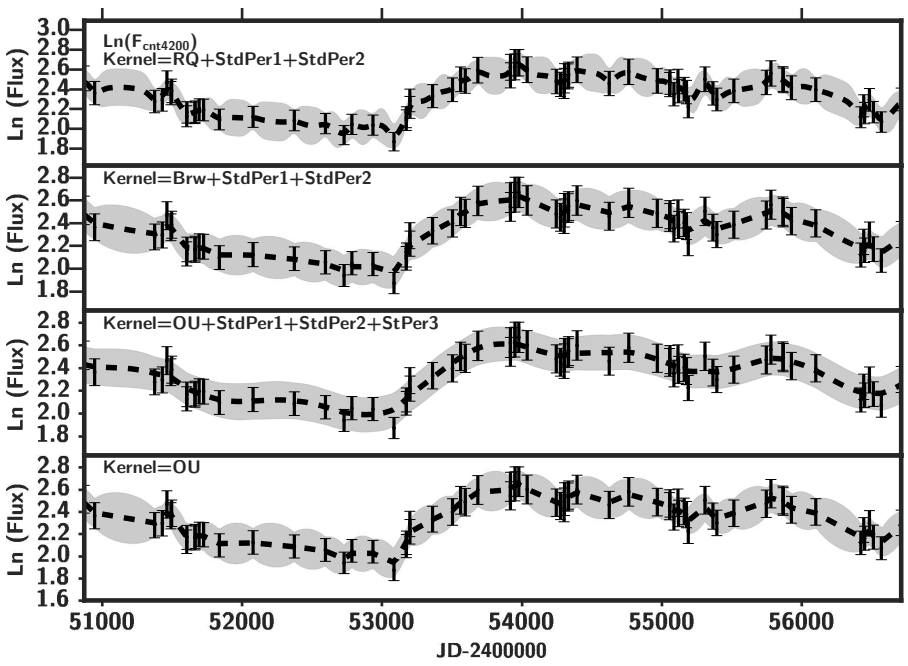

Fig. 4 The same as in Figure 3 but for the continuum at 4200 Å. Note that modeling was possible only with two periodic kernels.

4 Conclusions

We have performed a set of GP modeling (Table 1) of the continua at 4200, 5100 Å and the Hγ emission line light curves of E1821+643. Following direction of mixed covariance stochastic modeling of AGN light curves, we used composite GP models consisting of Ornstein - Uhlenbeck, the squared exponential, the rational quadratic, Brownian and non-stationary – periodic kernels. This allows us to quantify periodic signals in the light curves.

We found three strong signals with periods of ~ 12 yr, ~ 6 yr, and 4.8 yr (averaged values over all models). The two largest periods are in a harmonic relationship, which indicates their common physical origin. Analyzing the scenario with orbital motion of bright spots within the accretion disk, we found that t_{dyn} scales corresponding to the radii of origin of the Hβ and Hγ lines are almost equal to the two largest periods detected by GP models. However, the bright spot motion is not favored because any information about periodic signals is vanished from the Hβ line. Since the Hβ line arises at larger radius than Hγ, it seems that here some chaotic processes (like outflow) are presented that are destroying all periodic signals.

The third period of 4.8 yr is incommensurate with respect to the two largest periods, suggesting its different physical origin (such as flares at the radius of 2 ld within the accretion disk of the system).

So we propose that two largest periods correspond to the mutual dynamical interaction of two objects at least. Also, we analyzed the subcenario if these two objects are two kicked merging black holes. In such situation, we associated period of ~ 12 yr with the precession of orbital angular momentum of the system and the precession of the sum of two black holes' spins during the infall. The orbital period of black hole within this system can be associated with ~ 6 yr. In such setting, the rotational period of black hole would be nearly $\frac{7.4}{\cos\theta}$ yr, where θ is half-angle of the precession cone.

Acknowledgements This work was supported by the Ministry of Education and Science of Republic of Serbia through the project Astrophysical Spectroscopy of Extragalactic Objects (176001) and RFBR (grants N12-02-01237a, 12-02-00857a, 12-02-01237a,N15- 02-02101).

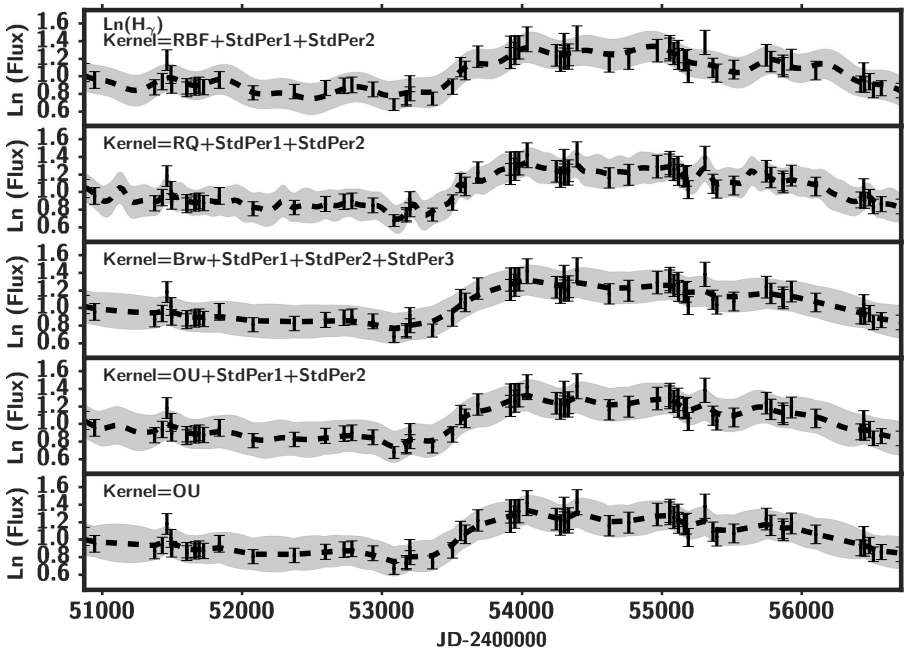

Fig. 5 The same as in Figure 3 but for the H_γ emission line. Note that stationary kernels composites includes only two periodic kernels.

References

Ackermann, M., Ajello, M., Albert, A., Atwood, W. B. et al., 2015, Astrophys. J. Lett., 813, 2, L41

Andrae, R., Kim, D. W., Bailer-Jones, C. A. L., 2013, å, 554, 137

Barausse, E., & Rezzolla, L. 2009, Astrophys. J. Lett., 704, L40

Bogdanović, T., Reynolds, C. S., & Miller, M. C. 2007, Astrophys. J. Lett., 661, L147

Bon, E., Jovanović, P., Marziani, P., Shapovalova, A. I. et al., 2012, Astrophys. J., 759, id. 118

Campanelli, M., Lousto, C. O., Zlochower, Y., & Merritt, D. 2007, Phys. Rev. Lett., 98. id231102

Durrande, N., Hensman, J., Rattray, M., & Lawrence, N. D. 2016, Peer J Computer Science 2:e50 https://doi.org/10.7717/peerj-cs.50

Fan, J. H., Lin, R. G., Xie, G. Z., Zhang, L. et al., 2002, Astron. Astrophys., 381, 1

Guilbert, P. W., Fabian, A. C., & Rees, M. J. 1983, Mon. Not. R. Astron. Soc.,205, 593

Gonzalez, J. A., Hannam, M. D., Sperhake, U., Brügmann, B., & Husa, S. 2007, Phys. Rev. Lett., 98. id. 231101

Graham, M. J., Djorgovski, S. G., Stern, D., Glikman, E. et al., 2015a, Nature, 518, 74

Graham M. J., Djorgovski, S. G., Stern, D.,Drake, A. J. et al., 2015b, Mon. Not. R. Astron. Soc., 453, 1562

Hagen-Thorn, V. A., Larionov, V. M., Jorstad, S. G., & Larionova, E. G. 2002, Astron. J., 124, 3031

Hughes, S. 2003, Annals of Physics, 303, 142

Jeffreys, H. 1961, Theory of Probability, 3rd ed. Oxford Classic Texts in the Physical Sciences. Oxford Univ. Press, Oxford. MR1647885

Table 1 Comparison of light curve models without heteroscedastic errors, using Bayes factor. In Lc column are given the light curves, used models are given in column M. Number of parameters used in each model are given in column NP, while inferred periods from models are given in columns Per_1, Per_2, and Per_3. LBF column stands for Bayes factor, ML column stands for marginal log likelihoods of models, S column stands for periodicity ratio of model, Ch column stands for the order of model based on LBF. In MP row are given averaged periods (in unit of days) from all models, while the brackets denote averaged periods in the units of years.

Lc	M	NP	Per_1 [*day*]	Per_2 [*day*]	Per_3 [*day*]	ML	LBF	S	Ch
Cnt_{5100}	$\mathrm{M_{OU}}$[a]	3	-	-	-	-125.76	-	-	-
	$\mathrm{PM_{OU}}$[b]	9	4829	2345	-	-133.56	7.8	1.23	1
	$\mathrm{M_1}$[c]	12	4857	2344	1628	-131.62	5.86	1.00	2
	$\mathrm{M_2}$[d]	13	3498	2363	1749	-131.04	5.28	1.02	3
	$\mathrm{M_3}$[e]	11	3787	1758	-	-126.87	1.1	1.02	4
Cnt_{4200}	$\mathrm{M_{OU}}$	3	-	-	-	-63.41	-	-	-
	$\mathrm{PM1_{OU}}$[f]	12	3852	1163	1860	-66.36	2.95	1.0	2
	$\mathrm{M_{22}}$[g]	9	4894	2372	-	-69.73	6.32	1.85	1
	$\mathrm{M_3}$	8	4028	1860	-	-63.9	0.49	1.44	Weak
H_γ	$\mathrm{M_{OU}}$	3	-	-	-	-56.75	-		
	$\mathrm{PM_{OU}}$	9	4717	2103	-	-58.92	2.2	1.2	3
	$\mathrm{M_{11}}$[h]	9	4978	2159	-	-62.06	5.31	1.00	1
	$\mathrm{M_{22}}$	10	5099	2093	-	-61.89	5.14	1.1	2
	$\mathrm{M_3}$	11	4420	1907	-	-57.69	0.93	1.13	Weak
MP			4451 (12.2)	2130 (5.8)	[i]1746 (4.8)				

[a] OU model of LC are considered as based model

[b] $\mathrm{PM_{OU}}$ assumes $\mathrm{OU} + \sum_{\mathrm{i}=1,2} \mathrm{StdPer_i}$

[c] $\mathrm{M_1}$ assumes Eq. 1

[d] $\mathrm{M_2}$ assumes Eq. 2

[e] $\mathrm{M_3}$ assumes Eq. 3

[f] $\mathrm{PM1_{OU}}$ assumes $\mathrm{OU} + \sum_{\mathrm{i}=1,3} \mathrm{StdPer_i}$

[g] $\mathrm{M_{22}}$ assumes $\mathrm{RQ} + \sum_{\mathrm{i}=1,2} \mathrm{StdPer_i}$

[h] $\mathrm{M_{11}}$ assumes $\mathrm{SE} + \sum_{\mathrm{i}=1,2} \mathrm{StdPer_i}$

[i] Period of 1163 days is not taken into account, since it is beyond two sample standard deviation below the mean of Per_2.

Table 2 Comparison of light curve models with three periodic components using Bayes factor. Subscript $_{het}$ stands for modeling with heteroscedastic errors.

Lc	M	NP	Per_{1het} [day]	Per_{2het} [day]	Per_{3het} [day]	ML_{het}	LBF_{het}	S_{het}
Cnt_{5100}	M_{OU}[a]	2	-	-	-	119.62	-	-
	PM_{OU}[b]	8	3565	2810	1151	110.8	-8.22	0.71
	M_1[c]	11	4435	-	-	274.896	155.28	3.3
	M_2[d]	12	4472	1731	1989	112.72	-6.89	0.7
	M_3[e]	10	4827	4721	2252	110.59	-9.02	0.99
Cnt_{4200}	M_{OU}	2	-	-	-	105.76	-	-
	PM_{OU}[b]	8	3828	1833	1151	-101.09	-4.763	0.53
	M_1[c]	11	3847	1847	1149	100.76	-5.03	1.48
	M_2[d]	12	4910	1158	-	100.9	-4.86	1.2
	M_3[e]	10	3796	1154	-	104.2	-1.56	0.36
H_γ	M_{OU}	2	-	-	-	31.37		
	PM_{OU}[b]	8	4978	2167	-	26.04	-5.33	0.99
	M_1[c]	11	4997	2167	-	26.04	-5.33	1.0
	M_2[d]	12	4903	1962	1154	25.11	-6.26	0.9
	M_3[e]	10	5006	2202	1551	25.9	-6.3	1
MP			4466 [i]	2159	1485			
			(12.2)	(5.92)	(4.07)			

[a] OU model of LC are considered as based model

[b] PM_{OU} assumes OU + $\sum_{i=1,3}$ $StdPer_i$

[c] M_1 assumes Eq. 1

[d] M_2 assumes Eq. 2

[e] M_3 assumes Eq. 3

[i] Period of 4435 days is not taken into account, due to large ML and LBF values.

Kass, R. E., & Raftery, A. E. 1995, Journal of the American Statistical Association, 90, 773

Kelly, B. C., Sobolewska, M., Siemiginowska, A., 2011, Astrophys. J., 730, 1, id. 52, 20

Kelly, B. C., Becker, A. C., Sobolewska, M., Siemiginowska, A., Uttley, P., 2014, Astrophys. J.788, 1, id. 33, 18

Kozlowski, S, 2016, Mon. Not. R. Astron. Soc.459, 3, 2787

Lainela, M., Takalo, L. O., Sillanpää, A., Pursimo, T. et al., 1999, Astrophys. J., 521, 561

Lobanov, A. P. & Roland, J. 2002, 6th European VLBI Network Symposium on New Developments in VLBI Science and Technology, 121

Lomb, N. R. 1976, Astrophys. J. Suppl. Ser., 39, 447

Lousto, C. O., & Zlochower, Y. 2009, Phys. Rev. D, 79, 064018

McKernan, B., Ford,K.?E.?S., Kocsis, B., Haiman, Z., 2013, Mon. Not. R. Astron. Soc., 432,1648

Mortier, A., Faria, J. P., Correia, C. M., Santerne, A., & Santos, N. C. 2015, Astron. Astrophys., 573, A101

Nipoti, C., & Binney, J. 2015, Mon. Not. R. Astron. Soc., 446, 1820

Noble, S. C., Mundim, B. C., Nakano, H., Krolik, J. H. et al., 2012, Astrophys. J., 755, 1, id. 51, 24

Pancoast, A., Brewer, B. J., Treu, T., Park, D. et al., 2014,Mon. Not. R. Astron. Soc., 445, 3073

Popović, L. Č., 2012, New Astron. Rev., 56, 74

Rasmussen, C. E., & Williams, C. 2006, Gaussian Processes for Machine Learning, the MIT Press

Robinson, A., Young, S., Axon, D. J., Kharb, P., & Smith, J. E. 2010, Astrophys. J. Lett., 717, 122

Rieger, F. M. 2004, Astrophys. J. Lett., 615, L5

Shapovalova, A. I., Popović, L. Č., Chavushyan, V. H., Burenkov, A. N. et al., 2016, Astrophys. J. Suppl. Ser., 222, id. 25

Sillanpää, A., Haarala, S., Valtonen M. J., Sundelius, B., & Byrd, G. G. 1988, Astrophys. J., 325, 628

Sundelius, B., Wahde, M., Lehto, H. J., &Valtonen, M. J. 1997, Astrophys. J., 484, 180

Valtonen, M. J., Lehto, H. J., Nilsson, K., Heidt, J. et al., 2008, Nature, 452, 851

Vaughan, S., Uttley, P., Markowitz, A. G., Huppenkothen, D. et al., 2016, Mon. Not. R. Astron. Soc., 461, 3145

Vlachos, M., Yu, P, Castelli, V., 2005, In: Kargupta, H., Srivastava, J., Kamath, C., Goodman, A. (eds.) Proceedings of the 2005 SIAM International Conference on Data Mining, 449

Volvach, A. E., Volvach, L. N., Larionov, M. G., Aller, H. D., Aller, M. F. 2007, Astronomy Reports, 51, 450

Zu,Y., Kochanek,C.S., Koz?owski,S., Udalski,A., 2013, Astrophys. J., 765, 2, id. 106, 7

This manuscript was prepared with the AAS LaTeX macros v5.2.